8988 *Biochemistry* **2010,** *49,* 8988–8998
DOI: 10.1021/bi100537f

BIOCHEMISTRY
including biophysical chemistry & molecular biology
Article

NmerA of Tn*501* Mercuric Ion Reductase: Structural Modulation of the pK_a Values of the Metal Binding Cysteine Thiols[†,‡]

Richard Ledwidge,[§,⊥] Baoyu Hong,[§] Volker Dötsch,[∥] and Susan M. Miller*[,§]

[§]*Department of Pharmaceutical Chemistry, University of California, San Francisco, 600 16th Street, San Francisco, California 94158-2517, and* [∥]*Institute of Biophysical Chemistry, Goethe University, Max-von-Laue Strasse 9, 60438 Frankfurt, Germany.* [⊥]*Present address: Office of Biotechnology Products, Division of Therapeutic Proteins, Food and Drug Administration, 29 Lincoln Dr., Building 29A, Room 2C22, Bethesda, MD 20892.*

Received April 9, 2010; Revised Manuscript Received September 8, 2010

ABSTRACT: To avoid nonspecific and/or undesirable binding and reactivity of metal ions with cellular components, organisms have evolved metal-specific systems for trafficking proteins. Although systems differ, those handling soft metal ions such as Hg^{2+}, Cu^{+}, Zn^{2+}, etc., all utilize heavy metal-associated (HMA) proteins and domains of ~70 amino acids with a conserved GMXCXXC motif in a $\beta\alpha\beta\beta\alpha\beta$ structural fold. While the conserved cysteines define a common metal binding site in these proteins, other structural features must be utilized to create metal ion, protein partner, and contextual specificities. This paper presents initial structure−function studies of the N-terminal HMA domain (NmerA) of Tn*501* mercuric ion reductase (MerA) aimed at identifying structural features critical to its role in facilitating efficient transfer of Hg^{2+} to the MerA catalytic core for reductive detoxification. First, NMR solution structures of reduced and Hg^{2+}-bound forms of NmerA are presented that allow definition and comparison of the structure of the metal binding loop in the two states. Structural differences between the two forms are compared with differences observed in three HMA domains with different metal ion and functional contexts. Second, analyses of the UV absorbance properties of wild-type, Cys11Ala, and Cys14Ala forms of NmerA are presented that provide assignments of the pK_a values for the two cysteine thiols of the metal binding motif. Third, results from ^{13}C NMR studies with wild-type and Y62F NmerA labeled with [β-^{13}C]cysteine are presented that define a role for Tyr62 in modulating the pK_a values of the cysteine thiols.

At elevated concentrations, metal ions pose significant challenges to living organisms because of the numerous opportunities for unwanted binding and/or catalytic reactivity with molecules in the cellular milieu (*1*, *2*). In response, trafficking systems that regulate the intracellular concentration and flow of metal ions have evolved with components including membrane-bound metal ion influx and efflux pumps, metallochaperones that specifically incorporate metal ions into target proteins, metal ion sequestration proteins, and occasionally metal ion reductases that catalyze reduction of metal ions to a less deleterious form (*3*−*9*). Unlike metalloproteins in which the metal ions provide structural or catalytic function to the protein, metal trafficking proteins interact transiently with their cognate metal ions as they transport them between or through cellular compartments. With metallochaperones and storage proteins like metallothioneins, the interactions are state-dependent in that they form stable interactions until the metal ion is transferred to a specific partner protein. With membrane transporters and reductases, the interactions with metal ion need to be completely transient. Elucidating the structural and catalytic features of proteins that lead to stable versus transient metal interactions is essential for understanding metal ion mobility and the pathways for metal ion toxicity.

Our studies focus on mercuric ion reductase (MerA)[1], the key enzyme of bacterial mercury detoxification pathways that rapidly reduces Hg^{2+} to Hg^0 (*5*, *6*). Hg^{2+}, a metal ion with no known biological function, has a very high affinity for dithiols [K_{form} for $Hg(SR)_2 \geq 10^{40}$ M^{-2}] but can also undergo rapid exchange of one thiol ligand for another (*2*, *10*), suggesting a general mode of Hg^{2+} toxicity through pleiotropic interactions with proteins in cells (*2*). Catalyzing the transformation to monatomic Hg^0 provides an effective means of eliminating the dangers posed by Hg^{2+} to a single-cell organism because Hg^0 has low aqueous solubility and

[†]This work was supported by grants from the National Science Foundation (MCB-9982576 to S.M.M.) and the Department of Energy, Office of Science (DE-FG03-01ER63087 to S.M.M.).

[‡]NMR data for determination of the reduced (BMRB entry 16207) and Hg-bound (BMRB entry 16208) NmerA structures have been deposited with the Biological Magnetic Resonance Bank. Coordinates for reduced NmerA (entry 2KT2) and the HgNmerA complex (entry 2KT3) structural models have been deposited in the Protein Data Bank.

*To whom correspondence should be addressed. Phone: (415) 476-7155. Fax: (415) 502-8298. E-mail: smiller@cgl.ucsf.edu.

[1]Abbreviations: catalytic core, amino acids 1 and 96−561 of Tn*501* MerA; C11A, Cys11Ala NmerA; C14A, Cys14Ala NmerA; DTNB, 5,5′-dithiobis(2-nitrobenzoic acid); DTT, dithiothreitol; FAD, flavin adenine dinucleotide; FHSQC, fast heteronuclear single-quantum coherence; H17N, His17Asn NmerA; HEPES, 4-(2-hydroxyethyl) piperazine-1-ethanesulfonic acid; $Hg(TNB)_2$, mercuric bis(thionitrobenzoate); HMA, heavy metal-associated; IAM, iodoacetamide; IPTG, isopropyl β-D-1-thiogalactopyranoside; KP_i, potassium phosphate buffer; LB, Luria-Bertani; MerA, mercuric ion reductase; NADPH, reduced nicotinamide adenine dinucleotide phosphate; NEM, *N*-ethylmaleimide; NmerA, N-terminal amino acids 1−69 of Tn*501* MerA; NOE, nuclear Overhauser effect; NOESY, nuclear Overhauser and exchange spectroscopy; PDB, Protein Data Bank; Tn*501*, transposon 501; TOCSY, total correlation spectroscopy; Y62F, Tyr62Phe NmerA.

 Published on Web 09/09/2010

little affinity for cellular ligands, allowing it to diffuse passively out of the cell (*11*−*13*).

MerA proteins are typically comprised of a multidomain catalytic core and one or two repeats of a small N-terminal domain (NmerA) (*5*). The catalytic core from the Tn*501* operon, which is homologous with the glutathione reductase family of FAD-containing disulfide oxidoreductases (*14*−*17*), has been extensively characterized (*5*, *18*−*26*). In this homodimeric protein of ca. 50 kDa monomers, FAD mediates the transfer of electrons between NADPH and Hg^{2+} bound to an adjacent pair of cysteine thiols (C136 and C141) in the buried active site, while a second pair of cysteines (C558 and C559) on the C-terminal tail mediates transfer of Hg^{2+} from other protein and small molecule thiols in solution to the active site cysteines through a ligand exchange mechanism (*25*, *26*). The N-terminal domain of ∼70 residues, NmerA, shares sequence homology with heavy metal-associated (HMA) trafficking proteins such as metallochaperones, soluble domains of membrane-bound metal ion transporters, and soluble metal ion receptors that exhibit a $\beta\alpha\beta\beta\alpha\beta$ fold with a conserved GMXCXXC metal binding motif (*6*, *27*, *28*). Using separately cloned core and NmerA constructs, we previously demonstrated the ability of NmerA to facilitate the acquisition of Hg^{2+} from other bulky thiol-containing compounds, including proteins, and its efficient transfer to the catalytic core for reduction (*27*, *29*). With this intermediary role, the structure of NmerA must have features that favor formation of its Hg^{2+} complex over those of other proteins and cellular thiols, as well as features that enhance the rapid transfer of Hg^{2+} to the core. In this paper, we present initial structure−function studies to explore these features. First, we describe the changes we observe in the NMR-derived solution structure of reduced NmerA upon binding of Hg^{2+} and discuss the similarities and differences with those observed in other reduced and metal-bound HMA domains with different physiological roles. Second, we present a combination of UV−visible and ^{13}C NMR studies of wild-type and several mutated forms of NmerA to evaluate the ability of two conserved residues, Tyr62 and His17, to modulate the pK_a values of the thiols of the metal binding cysteines, Cys11 and Cys14.

EXPERIMENTAL PROCEDURES

Materials. Reagents were purchased from Sigma or Aldrich. [^{15}N]Ammonium chloride, [$^{13}C_6$]-D-glucose, and [3-^{13}C]-L-cysteine were purchased from Isotec (Sigma-Aldrich).

NmerA Mutagenesis. Single mutations were introduced into NmerA following the QuikChange (Stratagene) mutagenesis kit protocols with appropriate primers. The following mutated proteins were generated: C11A, cysteine 11 to alanine; C14A, cysteine 14 to alanine; H17N, histidine 17 to asparagine; and Y62F, tyrosine 62 to phenylalanine. All mutations were verified by DNA sequencing.

Catalytic Core Purification, NmerA Purification, and Formation of the HgNmerA Complex. Purification of catalytic core and NmerA proteins and formation of the Hg−NmerA complex were performed as previously described (*27*). Thiol titrations were performed using DTNB as previously described (*27*).

Overexpression of ^{15}N-Labeled and ^{13}C- and ^{15}N-Labeled NmerA. NmerA, previously cloned from the Tn*501 merA* gene,[2] was expressed in BL21(DE3) pLys cells as previously described (*27*). To obtain proteins labeled for NMR structural studies, a 50 mL culture was grown in LB medium overnight at 37 °C and centrifuged for 5 min at 8000*g*. Cell pellets were suspended in 40 mL of uniformly ^{15}N-labeled or ^{13}C- and ^{15}N-labeled minimal M9 medium (6.8 g/L Na_2HPO_4, 3 g/L KH_2PO_4, 0.5 g/L NaCl, 1 g/L $^{15}NH_4Cl$, 2 g/L [$^{13}C_6$]-D-glucose, 2 mM $MgSO_4$, and 0.1 mM $CaCl_2$) containing 50 mg/L ampicillin and 34 mg/L chloramphenicol. A 20 mL suspension was used to inoculate 1 L of culture. Bacteria were grown to an OD_{600} of 0.8−1.0 and induced with 400 μM IPTG for 4 h at 37 °C. Cells were harvested by centrifugation (8000*g*) and frozen at −80 °C. Protein was purified as previously described (*27*).

Site-Specific ^{13}C-Labeled NmerA. The protocol of Cheng et al. (*30*) was used to generate NmerA labeled with ^{13}C at the β-carbon of cysteine. The ^{13}C-labeled protein was prepared by addition of [3-^{13}C]cysteine (60 μg/L) to our growth medium at the time of induction. The extent of labeling was not quantified. Qualitatively, the ^{13}C label at both cysteines could be detected in a quick two-dimensional ^{13}C HSQC experiment using just two scans with protein concentrations of ≥200 μM. However, the amount of incorporation varied from preparation to preparation.

Sample Preparation for NMR Structure Determination. Purified ^{15}N-labeled or ^{13}C- and ^{15}N-labeled NmerA was dialyzed against 10 mM HEPES (pH 7.0), concentrated to a small volume (0.25 mL), and exchanged with 10 mM deuterated HEPES (pH 7.0) by several concentration−wash cycles. HEPES buffer was chosen because the NMR signals exhibited their highest sensitivity when determined on the Bruker 500 MHz Avance NMR instrument equipped with a triple-resonance cryoprobe. The concentration of NmerA in the NMR tube was between 1 and 2 mM with 10% D_2O. For the reduced NmerA structure determination, 5 mM deuterated DTT was added to the sample. Sample preparation for determination of the Hg^{2+}-bound NmerA (HgNmerA) structure was identical to that for reduced NmerA with the exception that DTT was omitted from the sample. For experiments that required 100% D_2O, i.e., ^{13}C-edited NOESY, NmerA samples (reduced or Hg^{2+}-bound) in 10 mM deuterated HEPES were concentrated to 0.6 mL, lyophilized overnight, and redissolved in 0.6 mL of 100% D_2O.

NMR Spectroscopy and Structure Calculations. All experiments were performed on the Bruker 500 MHz Avance NMR instrument equipped with a triple-resonance cryoprobe at 303 K. Two-dimensional $^1H-^{15}N$ FHSQC spectra were used as a starting point in structure determination. ^{15}N-resolved three-dimensional TOCSY-HSQC and NOESY-HSQC experiments and ^{13}C-edited NOESY experiments were all performed with mixing times of 60 ms (*31*). Backbone and side chain resonance assignments were made using three-dimensional HNCA, CBCACONH, CCCONH, HBHACONH, and HCCONH experiments (*32*−*34*). HNHA experiments were performed to determine $^3J_{HNH\alpha}$ coupling constants that were used to obtain ϕ torsion angle constraints (*35*). Stereospecific assignments of methyl groups of valine and leucine were obtained by the procedure of Neri et al. (*36*). Water suppression was achieved through use of the WATERGATE sequence (*37*). All experiments were conducted and processed using standard XWINNMR software and analyzed using XEASY (*38*).

Structure calculations were performed with DYANA (*39*). The subroutine CALIBA in DYANA was used to convert cross-peak volumes of NOESY peaks into distance constraints. Coupling constants obtained in the HNHA experiment were used to determine backbone dihedral angle constraints using the subroutine

[2]The Tn*501* NmerA sequence is MTHLKITGMTCDSCAA**H**VKEALEKVPGVQSALVSYPKGTAQLAIVPGTSPDALTAAVAGLG**Y**KATLADA. The conserved metal binding motif is underlined, and conserved residues His17 and Tyr62 are shown in boldface.

GRIDSEARCH in DYANA. For the HgNmerA complex structure, a Hg^{2+} ion was included by linking a new residue connected to a chain of dummy atoms with their van der Waals radii set to 0. The radius of the Hg^{2+} atom was set to 1.35 Å, and the sulfur atom radii were changed to 1.05 Å as typically seen in a $Hg(SR)_2$ bond (*40*, *41*). The subroutine ANNEAL in DYANA was used to calculate 100 random structures in 10000 steps. Twenty conformers with the lowest target function were energy minimized by restrained Cartesian molecular dynamics in explicit solvent (i.e., water) using a CNS (*42*) protocol and force field that accounts for electrostatic and van der Waals interactions (*43*). In the case of the Hg-bound structure, the mercury ion was modeled as previously described (*44*) by defining two Hg−S covalent bonds of 2.33 Å to the neighboring cysteine residues. Table S1 of the Supporting Information contains the structural statistics of the final ensemble of 20 NMR structures for each structure. Coordinates for these have been deposited in the Protein Data Bank (entry 2KT2 for NmerA and entry 2KT3 for the HgNmerA complex), and chemical shift data have been deposited in the Biological Magnetic Resonance Bank (entry 16207 for NmerA and entry 16208 for the HgNmerA complex).

The 20 energy-minimized conformers were used as the final family for structural analysis. The quality of our structure determinations was examined by analysis of the ϕ and ψ angles for all residues of the different conformers using PROCHECK. Between 88 and 100% of residues for each conformer had ϕ and ψ angles in the most favored regions of a Ramachandran plot and 0−12% in additionally allowed regions. Angles for either Asp12 or Ser13 typically were not found in most favored regions, most likely because of the small number of NOEs involving these residues.

^{13}C NMR pH Titrations. Samples for pH studies with wild-type (WT) and H17N, Y62F, C11A, and C14A mutant NmerA proteins labeled with ^{13}C at the β-carbon of cysteine were dialyzed twice against 4 L of 10 mM KP_i (pH 7.3) with 2 mM DTT. NmerA proteins for NMR pH studies were used at concentrations of 0.5−1 mM in the presence of 5 mM DTT. To test the reduced thiol stability, wild-type protein at a concentration of 0.89 mM was incubated at 25 °C in 50 mM KP_i and 5 mM DTT (pH 8.0). Aliquots were taken at 1 h intervals over a period of 8 h and separated from DTT by size exclusion chromatography (Econo-Pac 10DG columns with P6-DG), and the thiols were titrated using DTNB (*27*). No oxidation of the protein thiols occurred during the 8 h incubation.

^{13}C NMR pH titration experiments were performed using a Bruker 500 MHz Avance NMR instrument equipped with a triple-resonance cryoprobe at 303 K. Reduced [β-^{13}C]cysteine-labeled NmerA in 10 mM KP_i (pH 7.3) containing 10% D_2O and 5 mM DTT was used in pH titrations. The pH of the solution was adjusted via addition of aliquots of 1.0 M HCl or 1.0 M NaOH to the sample. The sample was filtered after every addition of acid or base. The pH was measured both before and after each acquisition, with the latter measurement used for data analysis. pH values were not adjusted for the concentration of D_2O. Chemical shifts in two-dimensional ^{13}C HSQC experiments were referenced to free [$^{13}C_5$]-L-methionine in an external reference NMR tube.

Spectrophotometric pH Titrations. Two methods were used for these studies. For both, we prepared unlabeled NmerA proteins by first concentrating them to ~0.5 mL, incubating them with 5 mM DTT for 20 min, and separating them from DTT by passage through a P2 gel filtration column. In the first method, the sample was exchanged into 10 mM KP_i (pH 7.3) during gel filtration and fractions containing WT or mutant NmerA were pooled and concentrated to ~50 μM for the titrations. Protein concentrations were determined from the A_{278} using an ε_{278} of 2.55 mM^{-1} cm^{-1} for WT NmerA and the C11A and C14A mutants and an ε_{278} of 1.25 mM^{-1} cm^{-1} for the Y62F mutant, which were determined by amino acid analysis of a spectrally characterized solution (*27*). [The A_{278} for all proteins remained constant (±1.3%) below pH 9.5 and began to increase systematically only at pH > 9.5.] Protein thiols were quantitated before titration using DTNB (*27*), and all proteins were fully reduced. In this method, the pH was adjusted, the sample was filtered, and the pH was measured exactly as in the NMR titrations. In the second procedure, proteins were exchanged into 5 mM sodium acetate (pH 5.0), concentrated to ~1.4 mM, and kept at 4 °C during the course of the experiment. Protein thiols in aliquots of the stock samples were determined using DTNB before, midway, and at the end of the titration and remained constant. For each pH, 0.025 or 0.04 mL of protein stock was diluted into 0.975 or 0.96 mL, respectively, of buffer using an overlapping series of 35 mM sodium citrate (pH 3−6.5), 35 mM sodium phosphate (pH 6.5−8.3 and 11.5−13), 70 mM sodium bicarbonate (pH 9.5−11), and 20 mM sodium pyrophosphate (pH 8.3−9.5) adjusted to a constant ionic strength of 210 mM with NaCl. To test the reduced thiol stability at high pH, the A_{240} was measured immediately after dilution into the highest-pH (~13) buffer, as well as several lower-pH buffers, and was found to remain stable in all cases for at least 10 min. Absorbance spectra were recorded in a Uvikon XL spectrophotometer with the temperature held at 25 °C.

Alkylation of C11A and C14A with N-Ethylmaleimide (NEM) and Iodoacetamide (IAM). To determine the accessibility of the two cysteine thiols, the rates of alkylation for the remaining thiol in each of the C11A and C14A mutants by NEM and IAM were determined at pH 6.5, which is below the pK_a value of the remaining thiol in both proteins (see below). For each, 100 μM protein was mixed with 100 μM NEM or IAM in 5 mM NaAc (pH 6.5) at room temperature in a total volume of 1.0 mL; 0.1 mL aliquots were removed ~0.5, 2, 4, 6, 8, and 10 min after mixing and diluted into 6 M guanidine hydrochloride (pH 8) containing 200 μM DTNB to measure residual thiols. In a control reaction, no change in the absorbance at 412 nm was observed over a period of 5 min for a solution of 10 μM thionitrobenzoate (TNB product in DTNB reaction) after addition of 10 μM NEM or IAM, indicating the reaction of TNB with NEM or IAM at these low concentrations is sufficiently slow that the TNB absorbance provides a good measure of the residual thiol concentration.

Data Fitting for pH Studies. Models describing one, two, and three noninteracting macroscopic ionizations (eqs 1−3) were used to determine macroscopic pK_a values using curve fit procedures in Kaleidagraph (Synergy)

$$\delta_{obs} = [\delta_a + \delta_b \times 10^{(pH - pK_a)}]/[1 + 10^{(pH - pK_a)}] \quad (1)$$

$$\delta_{obs} = [\delta_a + \delta_b \times 10^{(pH - pK_{a1})} + \delta_c \times 10^{(2\times pH - pK_{a1} - pK_{a2})}]/ [1 + 10^{(pH - pK_{a1})} + 10^{(2\times pH - pK_{a1} - pK_{a2})}] \quad (2)$$

$$\delta_{obs} = [\delta_a + \delta_b \times 10^{(pH - pK_{a1})} + \delta_c \times 10^{(2\times pH - pK_{a1} - pK_{a2})} + \delta_d \times 10^{(3\times pH - pK_{a1} - pK_{a2} - pK_{a3})}]/[1 + 10^{(pH - pK_{a1})} + 10^{(2\times pH - pK_{a1} - pK_{a2})} + 10^{(3\times pH - pK_{a1} - pK_{a2} - pK_{a3})}] \quad (3)$$

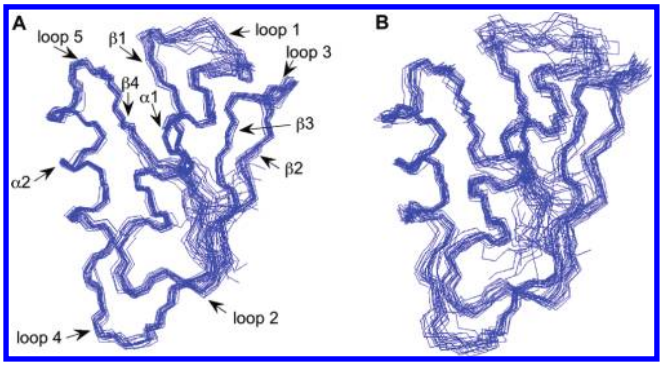

FIGURE 1: Bundles of the 20 lowest-energy structures calculated from NMR constraints for (A) reduced NmerA (PDB entry 2KT2) and (B) Hg-bound NmerA (PDB entry 2KT3), positioned in same orientation as in Figure 6A of ref *46*. Figures were prepared in MolMol (*63*).

where δ_{obs} is the observed chemical shift of the β-carbon of the NmerA cysteine and δ_i is the chemical shift for that carbon in each ionization state of the protein. For the spectrophotometric titrations, δ_{obs} corresponds to the observed absorbance (A_{240} or A_{293}), δ_i corresponds to the extinction coefficient (ε_{240} or ε_{293}) of each species at the monitored wavelength, and the right-hand side of each equation is multiplied by the total concentration of NmerA in the experiment.

RESULTS AND DISCUSSION

NmerA Structure Determination. As described in Experimental Procedures and the Supporting Information, we have determined the solution structures of the reduced and Hg^{2+}-bound forms of the 69-residue Tn*501* NmerA domain using conventional three-dimensional NMR techniques. While completing our structure calculations, a model was reported for the fold of the Hg^{2+}-bound form of MerAa (an identical 68-residue domain from the *Ralstonia metallidurans* CH34 MerA) that had been obtained using residual dipolar couplings and long-range methyl−methyl NOEs (*45*, *46*). As expected, the results are very similar, but there are some differences that we highlight here.

In the $^1H-^{15}N$ HSQC spectrum for reduced MerAa (Figure 5A of ref *45*), no backbone resonances were observed for residues 10−15, which comprise the key metal binding motif in the protein (*45*); however, peaks for all but one (Asp12) did appear in the spectrum for the HgMerAa complex (Figure 5B of ref *45*), allowing solution of the full structural model only for the metal-bound protein. In contrast to this, only one backbone resonance in the metal binding loop (Ser13) was missing in the $^1H-^{15}N$ FHSQC spectra for both reduced and Hg-bound NmerA (Figure S1 of the Supporting Information); thus, models for both forms of NmerA have been calculated and can be compared.

The reduced NmerA structure was obtained with high precision (Table S1 of the Supporting Information) as is evident in the bundle of the 20 lowest-energy conformers shown in Figure 1A. Fewer constraints for the HgNmerA complex (see the Supporting Information) resulted in a lower precision in the bundle of structures for the Hg-bound protein in Figure 1B. However, the root-mean-square deviation (rmsd) values for the HgNmerA model (Table S1 of the Supporting Information) are similar to those reported for the HgMerAa model which is also visually apparent by comparison of the bundle shown in Figure 1B with the similarly oriented bundle shown in Figure 6A of ref *46*. From this comparison, it can also be seen that the structural calculations from the data for the two different samples result in a very similar overall fold, but with two apparent differences. The orientation and alignment of the two α-helices, β-strands 1 and 4 (top left of the structure, Figure 1B), and loops 2 and 4 (bottom of structure) appear to be nearly identical in the two structures. However, β-strand 3 is visible to the left of β-strand 2 (right side of the structure, Figure 1B) in this orientation of the HgNmerA structure, whereas it is aligned behind β-strand 2 in the HgMerAa structure (*46*), resulting in a slightly different alignment of strands 2 and 3 relative to α-helix 1 and, more importantly, a slightly different positioning of loop 3 relative to the metal binding loop above it. In addition, the average position of the metal binding loop itself, although not very well-defined in either structure, appears to be bent back against the surface of the protein in the HgNmerA structure (Figure 1B) but more extended in the HgMerAa structure (*46*). These differences are consistent with the slightly different peak positions observed for some of the residues in these regions in the HSQC spectra for the two samples (Figure S1 of the Supporting Information and Figure 5A,B of ref *45*) and may reflect perturbations arising from differences in the experimental conditions of the two samples (both pH 7.0 but 10 mM HEPES and 30 °C here vs 50 mM Tris and 20−25 °C for MerAa).

Comparisons with Other HMA Domains and Proteins. The presence of a reasonably well-defined metal binding loop in both the reduced and metal-bound NmerA structures allows comparison of the changes that occur upon metal binding in this protein with other HMA domains and proteins. Focusing on NMR-derived solution structures of HMA domains available in the PDB, we discovered that structural changes occurring upon metal binding differ and correlate in an interesting manner with the different functions of the domains, but not necessarily with the specific metal ion. To illustrate this, Figure 2 compares the structures with and without metal for two pairs of proteins that bind different metal ions, NmerA (panel A) and MerP (*44*) (panel B) with and without Hg^{2+}, and Ccc2a (*47*) (panel C) and Atx1 (*48*) (panel D) with and without Cu^+. Within each pair, the first (NmerA and Ccc2a) is normally expressed as an appended domain of a larger protein to which it mediates transfer of the metal ion obtained from other sources. The second member of each pair (MerP and Atx1) is an independently expressed protein that must diffuse through a particular cellular compartment to acquire and transfer the metal ion from or to specific partners at different locations. Focusing first on NmerA (Figure 2A), which is normally appended to the catalytic core of MerA, we find the structures with and without Hg^{2+} overlay very closely with nearly identical secondary structures and only fairly small changes in the mean positions of the various loops, including the metal binding loop. In the Cu^+ binding homologue Ccc2a (Figure 2C), which is normally appended to an integral membrane copper transporter, the structural changes upon binding Cu^+ are even smaller, with almost no change in the position of the metal binding sulfurs.

In contrast to the very minor structural changes in the normally appended domains, both of the diffusible proteins [MerP and Atx1 (panels B and D of Figure 2, respectively)] undergo significant conformational changes in their metal binding loops and loop 3, which lies beneath and supports the metal binding loop in each case. In particular, the mean positions of the cysteine sulfurs change dramatically between reduced and metal-bound structures of these two. Notably, however, the placement of the cysteines in the two reduced proteins is quite different. In MerP, which is located in the periplasm (*6*), the cysteine sulfurs become

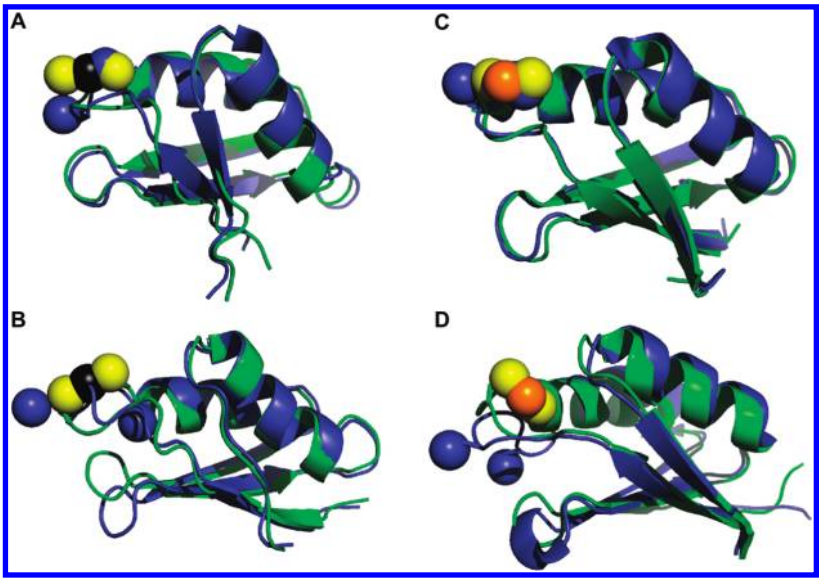

FIGURE 2: Comparison of structural changes upon metal binding in normally appended metal binding proteins (A) NmerA with and without Hg^{2+} [PDB entries 2KT3 (with Hg) and 2KT2 (without Hg)] and (C) Ccc2a with and without Cu^{+} [PDB entries 1FVS (with Cu) and 1FVQ (without Cu) (*47*)] vs free-standing metal binding proteins (B) MerP with and without Hg^{2+} [PDB entries 1AFJ (with Hg) and 1AFI (without Hg) (*44*)] and (D) Atx1 with and without Cu^{+} [PDB entries 1FD8 (with Cu) and 1FES (without Cu) (*48*)]. Mean structures were available in the PDB for Ccc2a with and without Cu^{+} and Atx1 with and without Cu^{+} but were calculated from the family of structures for NmerA with or without Hg and MerP with or without Hg using MolMol (*63*). To calculate the mean metal-bound structures, the metal ion had to be temporarily designated as a hydrogen atom attached to one of the sulfurs in each coordinate file and then redesignated as the metal ion in the mean structure. Mean structures were aligned in Chimera (*64*) and rendered in PyMOL (*65*). Reduced proteins are colored blue with cysteine sulfurs as blue spheres; metal-bound proteins are colored green with yellow cysteine sulfurs as spheres, Hg^{2+} as black spheres, and Cu^{+} as copper spheres.

well-separated in the absence of Hg^{2+}, with the first one in the motif folded out into solution and the second becoming deeply buried. Such a conformation is ideal for the oxidizing environment of the periplasm as it should decrease the likelihood of the cysteine pair becoming oxidized to a disulfide and losing its metal binding ability. In Atx1, which is located in the cytoplasm (*48*), the picture is quite different. In this case, both sulfurs become fully exposed in the absence of metal ion, which may be important for initiating or exiting from Cu^{+} transfer but interestingly also correlates with the lower risk of oxidation in the strongly reducing environment of the cytoplasm. A further difference between Atx1 and MerP is that the bound metal ion in MerP remains fairly exposed on the surface of the protein while that in Atx1 becomes completely buried. This again is consistent with their cellular locations because Atx1 needs to protect the bound Cu^{+} from attack by noncognate thiols as it diffuses through the thiol-rich cytoplasm, whereas MerP would encounter very few reduced thiols to attack its bound Hg^{2+} in the periplasm. Of interest, the bound metal ions in the normally appended NmerA and Ccc2a domains are also fairly exposed on their surfaces in spite of the fact that both of these domains are located in the cytoplasm. In this case, however, neither domain has to diffuse for an uncertain time or distance through the cytoplasm before transferring its metal ion to a cognate partner; rather, the transfers are intramolecular, leaving substantially less time for competition by other thiols.

In summary, while this is a limited analysis, two dominant types of structural changes occur in these domains upon binding metal ions that appear to be correlated with cellular function. (1) The magnitude of structural changes in the metal binding loops varies according to whether the domain is normally appended or diffusible. Minimal changes appear to be optimal for the appended "antennae" proteins that need to efficiently receive the metal ion from an external donor and pass it along to an intramolecular recipient, while larger changes occur in diffusible domains as a means of protecting one of their longer-lived alternative states from the "hostile" environment of their particular cellular compartment. (2) Burial of the bound metal ion appears to be a feature of diffusible cytoplasmic domains that need to protect the metal ion from attack by nonspecific ligands, while exposure of the metal ion is a feature of both appended and diffusible periplasmic domains in which the level of competition for the metal by nonspecific ligands is decreased because of either rapid intramolecular transfers or simply the absence of available ligands. Further analysis of what features regulate these structural changes and whether these properties are important for their in vivo function is needed.

Residues Important for NmerA Function. Although the exact roles of the HMA binding domains and proteins vary significantly, they all serve as intermediaries in the transfer of their cognate metal ions from one or more source sites (that are not well-defined in many cases) to a specific acceptor protein (*28*). In each case, the two cysteine thiols of the conserved GMXCXXC motif form the primary binding site for the heavy metal ion, which in this instance gives a 1:1 Hg^{2+} bis-thiolate complex of NmerA (*27*, *46*). Functionally, it has been shown that NmerA can acquire Hg^{2+} from other peptides (*49*) and protein Hg−dithiol complexes and deliver it efficiently to the catalytic core for reduction (*27*). Transfers of Hg^{2+} are known to occur through an associative mechanism with formation of transient three-coordinate complexes (*10*). In an associative mechanism, the cysteines of NmerA serve first as nucleophiles during the acquisition of Hg^{2+} from other dithiol complexes and then as leaving groups during the handoff to the catalytic core, similar to the alternating catalytic roles played by the nucleophilic thiol in cysteine proteases. To achieve optimal catalysis with this dual role, the pK_a of the thiol is typically lowered by the local environment of the enzyme from a value near 10 for the free

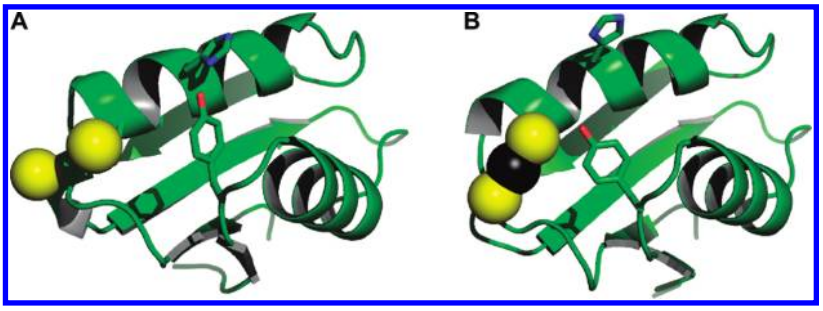

FIGURE 3: Two of the lowest-energy structures calculated for NmerA with and without Hg^{2+} showing alternative orientations of the cysteine sulfurs (yellow spheres) and the side chains of conserved residues Tyr62 and His17. (A) Reduced NmerA (PDB entry 2KT2, model 1) and (B) HgNmerA complex (PDB entry 2KT3, model 19). These two orientations define the extremes in the range of motion observed for the Tyr62 side chain in both the reduced and metal-bound structures. Figures were rendered in PyMOL (*65*).

amino acid to a value near or below the relevant physiological pH. This serves both to stabilize the thiolate anion as a leaving group and to increase the nucleophilicity because thiolates are 3−4 orders of magnitude more nucleophilic than their corresponding thiols (*50*, *51*). Ionizable residues that can participate in protonation and deprotonation of the cysteine thiols or other structural features that can stabilize the developing negative charge upon deprotonation are likely candidates for facilitating Hg^{2+} binding and exchange reactions.

The solution structure of NmerA in conjunction with sequence alignments suggests Tyr62 and His17 as residues that could participate in NmerA function by charge stabilization and/or protonation and deprotonation of the cysteine thiols (Figure 3). Tyr62 is uniformly conserved among NmerA domains (*6*) and is located on loop 5 juxtaposed to the metal binding loop. Tyr or Phe at this position is also very common among other families in the metal binding domain superfamily and is primarily postulated to serve a structural role by making hydrophobic contacts with the side chains of the methionine and second cysteine residues of the conserved GMXCXXC metal binding motif (*28*). Hydrophobic contacts between the phenyl ring of Tyr62 and the side chain of Met9 are also present in our structures of NmerA, supporting a similar structural role. However, a more direct interaction of the polar functional group with the thiols of the metal binding motif might also be relevant, as appears to be the case for the corresponding residue in the Cu^{+} metallochaperones (*28*). In that family, tyrosine is replaced uniformly by a lysine whose positively charged ammonium group lies near the Cu^{+} bis-thiolate center and is thought to stabilize the complex by neutralizing the negative (−1) charge (*28*, *48*). In both our reduced and Hg-bound NmerA structures, orientations of the side chain of Tyr62 with the OH group positioned near the imidazole ring of His17, near the sulfur of Cys14, or suspended between them are all found to satisfy the NMR constraints, suggesting this group may influence the chemical properties of the thiol(s). His17 is a uniquely conserved residue in NmerA sequences that is not found in any other "ferredoxin-like" metal binding protein (*6*, *28*), suggesting it is specifically relevant for NmerA function. As noted above, the NMR constraints suggest it can interact with the Tyr62 hydroxyl group, but as shown in Figure 3, its location one turn away from Cys14 along α-helix 1 also suggests a potential electrostatic interaction that could stabilize the Cys14 thiolate. To test the proposed roles of these conserved residues in NmerA function, we first evaluated the pH titration behavior of residues in and near the metal binding motif in the wild-type protein using a combination of ^{13}C NMR spectroscopy, UV absorption spectroscopy, and site-directed mutagenesis of the individual cysteines.

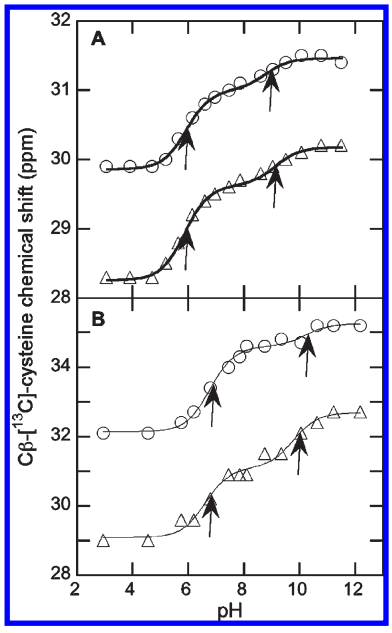

FIGURE 4: Changes in the ^{13}C NMR chemical shifts for the β-carbons of Cys11 (○) and Cys14 (△) as a function of pH for (A) reduced wild-type NmerA and (B) reduced Y62F mutant NmerA. All curves were fit to eq 2 for two ionizations; arrows denote approximate pK_a values (Table 1).

^{13}C NMR pH Titrations of Wild-Type NmerA. To determine the cysteine thiol pK_a values, we expressed NmerA in the presence of cysteine labeled with ^{13}C at the β-carbon and monitored the change in ^{13}C NMR chemical shift as a function of pH. ^{13}C at the β-carbon of cysteine has been shown to be a sensitive probe of ionization (*10*, *52*) and metal liganding of the thiol (*10*), as well as of ionizations in the vicinity of the thiol in a number of protein systems (*53*). The pH dependence of the chemical shifts for the Cys11 and Cys14 β-carbons of wild-type NmerA is shown in Figure 4A. The data for both Cys11 and Cys14 were best fit by a model with two macroscopic ionizations exhibiting pK_a values of ~6 and 9 (Table 1). The similarity in pK_a values observed for the β-carbons of both cysteines suggests they are reporting on the same ionizations.

Spectrophotometric pH Titrations of Wild-Type NmerA. To determine more directly whether the ionizations observed in the chemical shift data are due to ionization of the cysteine thiols, we examined the pH dependence of the UV absorbance at 240 nm where formation of cysteine thiolates gives an increase in absorbance

Table 1: pK_a Values Obtained from pH Titrations[a]

protein	Cys11 β-^{13}C chemical shift		Cys14 β-^{13}C chemical shift		absorbance at 240 nm[b]		absorbance at 293 nm[c]	
	pK_a	$\Delta\delta$[d] (ppm)	pK_a	$\Delta\delta$[d] (ppm)	pK_a	$\Delta\varepsilon_{240}$[e] (mM^{-1} cm^{-1})	pK_a	$\Delta\varepsilon_{293}$[e] (mM^{-1} cm^{-1})
WT (reduced)	5.92 ± 0.06	1.16	5.86 ± 0.04	1.37	6.40 ± 0.15	5.5		
	8.74 ± 0.16	0.44	9.10 ± 0.11	0.54	8.96 ± 0.45	2.6		
					11.33 ± 0.07	15.4	11.42 ± 0.03	4.9
WT (oxidized)	none detected		6.72 ± 0.08[f]	0.3				
					10.42 ± 0.03[f]	15.4	10.48 ± 0.03	4.3
C11A	NA[g]		7.34 ± 0.06	3.23	7.08 ± 0.13	5.8		
					11.16 ± 0.05	17.1	11.17 ± 0.03	5.0
C14A	8.00 ± 0.08	2.49	NA[g]		7.30 ± 0.13	3.0		
					11.02 ± 0.05	13.4	11.05 ± 0.03	4.1
H17N (reduced)	6.18 ± 0.08	1.33	6.23 ± 0.04	1.44	ND[h]		ND[h]	
	8.91 ± 0.27	0.41	9.38 ± 0.25	0.29				
Y62F (reduced)	6.80 ± 0.08	2.46	6.63 ± 0.15	2.0	6.94 ± 0.08	2.8		
	10.21 ± 0.34	0.6	9.78 ± 0.20	1.6	9.30 ± 0.13	3.3		
					11.20 ± 0.04	7.4	11.02 ± 0.05	2.2

[a]NMR titrations were performed at 30 °C and absorbance titrations at 25 °C. [b]Absorbance at 240 nm monitors formation of thiolates and tyrosine anions. [c]Absorbance at 293 nm monitors only formation of tyrosine anions. [d]All chemical shifts were downfield shifts. [e]All absorbance changes were increases. [f]Since Cys11 and Cys14 form a disulfide in oxidized NmerA, pK_a values observed by ^{13}C NMR represent ionization of other residues in the vicinity of the C14 β-carbon, and those observed by ΔA_{240} are for only tyrosines. [g]Not applicable. [h]Not determined.

with extinction coefficients ($\Delta\varepsilon_{240}$) typically ranging from 4000 to 6000 M^{-1} cm^{-1} in proteins (*54*, *55*). The ε_{240} observed during a direct pH titration of wild-type NmerA is shown in Figure 5A. The data fit best to a model involving three ionizations with pK_a values of ~6.4, 9.0, and 11.3 (Table 1). Essentially identical results were obtained in a separate experiment in which aliquots of a concentrated protein stock maintained at pH 5.0 were diluted into a series of buffers at a constant ionic strength (Figure S2A of the Supporting Information). The pK_a of 11.3 is assigned to the ionization of the two tyrosine residues (Y35 and Y62) as it exhibits a $\Delta\varepsilon_{240}$ typical for 2 equiv of tyrosine (*56*, *57*). Further evidence supporting this assignment includes the observation of a pK_a of 11.3 associated with a corresponding increase in A_{293} (Figure S3 of the Supporting Information and Table 1) that is characteristic of tyrosine anions but not thiolates (*56*, *57*), and also with the observation by A_{240} and A_{293} of only a single pK_a of ~10.5 in the pH titration of oxidized NmerA with its cysteine pair in a disulfide (Table 1). The other two pK_a values observed in the spectrophotometric titration (6.4 and 9.0) are similar to those observed in the ^{13}C NMR data, strongly suggesting that the two ionizations in the ^{13}C NMR experiment reflect the ionization of the cysteine thiols.

To verify this and determine if the two cysteines have distinguishing properties, we evaluated the spectrophotometric titration behavior of individual cysteine mutants C11A and C14A using both approaches. Consistent with the above assignments, the pH titrations for both mutants fit best to a model with only two ionizations (Figure 5B and Figure S2B of the Supporting Information), where the higher pK_a is again attributed to the tyrosine residues, based on the $\Delta\varepsilon_{240}$ and $\Delta\varepsilon_{293}$ values (Table 1), and the lower pK_a to the remaining cysteine thiol in each case. Using the first titration approach, a pK_a value of 7.1 ± 0.1 was observed in the C11A titration for the remaining Cys14, while a pK_a value of 7.3 ± 0.1 was observed in the C14A titration for Cys11 (Figure 5B and Table 1). Consistent with this, the second approach gave similar values of 7.0 ± 0.1 and 7.0 ± 0.2 for

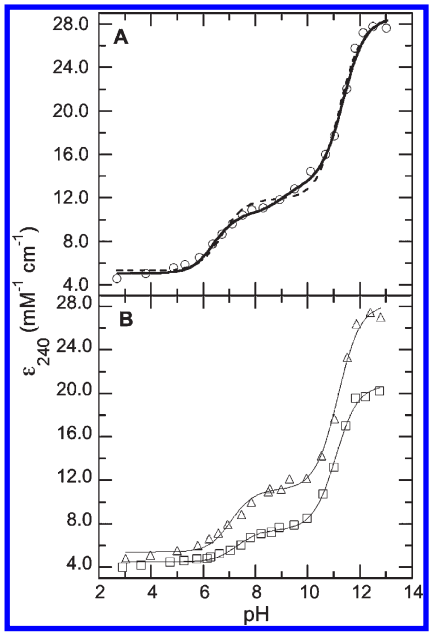

FIGURE 5: Absorbance of NmerA proteins at 240 nm as a function of pH. (A) Wild-type NmerA at 36.8 μM (○). The solid line shows a fit to three ionizations (eq 3). The dashed line that deviates in midregion shows a fit to two ionizations (eq 2). (B) C11A at 40.8 μM (△) and C14A at 44.7 μM (□), both fit to two ionizations (eq 2).

Cys14 in replicate C11A titrations, and values of 7.45 ± 0.15 and 7.54 ± 0.16 for Cys11 in replicate C14A titrations (Figure S2B of the Supporting Information). Similarly, only a single pK_a was detected by ^{13}C NMR in pH titrations of β-[^{13}C]Cys-labeled C11A (pK_a ~ 7.3) and C14A (pK_a ~ 8.0) mutants (Table 1 and Figure S4A of the Supporting Information). Comparison of the individual pK_a values for the two mutants to the two pK_a values observed in wild-type NmerA indicates that the absence of the second thiol in each case causes a significant perturbation in the pK_a value of the remaining thiol, making it difficult to assign

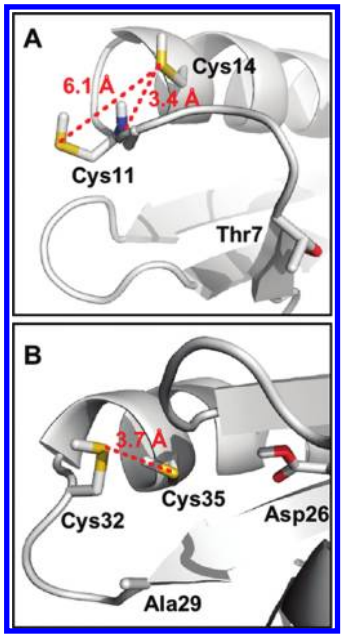

FIGURE 6: Comparison of CXXC motifs and the preceding $\beta-\alpha$ loops in NmerA and *E. coli* thioredoxin. (A) NmerA (PDB entry 2KT2, model 1). (B) *E. coli* thioredoxin (PDB entry 1XOB, model 1). Structures were rendered in PyMOL (*65*) and labeled in Kaleidagraph.

the wild-type values to the individual cysteines on this basis alone. However, the absorbance changes ($\Delta\varepsilon_{240}$) for the two Cys to Ala mutants differ as they do for the two phases in the titration of the wild-type protein. From the titrations of C11A, the $\Delta\varepsilon_{240}$ for Cys14 is 5.65−5.9 mM^{-1} cm^{-1}, and from the titrations of C14A, the $\Delta\varepsilon_{240}$ for Cys11 is 3.0−3.3 mM^{-1} cm^{-1} (Figure 5B and Figure S2B of the Supporting Information). Returning to the wild-type titration in Figure 5A, we can see that the $\Delta\varepsilon_{240}$ associated with the lower pK_a [5.5 mM^{-1} cm^{-1} (Table 1)] is close to that for Cys14 in C11A while the $\Delta\varepsilon_{240}$ associated with the second pK_a [2.6 mM^{-1} cm^{-1} (Table 1)] is close to that of Cys11 in C14A. These distinctions provide strong evidence for assignment of the lower pK_a of 5.9−6.4 in wild-type NmerA to Cys14 and of the higher pK_a of ∼9.0 to Cys11, which is consistent with the lower pK_a (7.0−7.3) observed for Cys14 and the higher pK_a (7.3−8.0) observed for Cys11 in the C11A and C14A mutants, respectively. In addition, these assignments are consistent with the observation of a lower pK_a of ∼5.5 for the second cysteine (C17) of the CXXC motif in the related Hg-binding protein MerP and a higher pK_a of ∼9.2 for the first cysteine (C14) in that motif (*58*).

To further verify the assignment of the observed pK_a values to successive ionizations of the two thiols in wild-type NmerA, we also considered examining the order of alkylation of the two cysteines at the pH of the lower pK_a (∼6) using sequential additions of 1 equiv of *N*-ethylmaleimide (NEM) followed by excess iodoacetamide (IAM). To assess the validity of this approach, we first compared the rates for alkylation of Cys14 in C11A and of Cys11 in C14A with both reagents at pH 6.5. At this pH, Cys14 in C11A should be more deprotonated than Cys11 in C14A because it has a lower pK_a so we would expect the rate for alkylation of Cys14 to be slightly faster than that of Cys11 if both are equally accessible. In contrast, Cys14 (in C11A) was found to react ∼8-fold more slowly than Cys11 (in C14A) with IAM and ∼14-fold more slowly with NEM, indicating Cys14 is significantly less accessible than Cys11 to alkylation reagents and precluding use of this method to evaluate the relative pK_a values in wild-type NmerA.

Table 2: Comparison of ^{13}C $\Delta\delta$ Values for Cysteines in *E. coli* Thioredoxin versus NmerA

	E. coli Trx		NmerA[a]	
	Cys32	Cys35	Cys11	Cys14
pK_{a1}	7.4[b] 7.6[c]	7.7[b] 7.6[c]	5.9	5.9
$\Delta\delta_1$ (ppm)	1.6[b] 1.44[c]	0.5[b] 0.43[c]	1.16	1.37
pK_{a2}	9.7[b] 9.9[c]	∼10.3[b] 9.9[c]	8.7	9.1
$\Delta\delta_2$ (ppm)	1.9[b] ∼2.2[c]	∼0.8[b] 0.63[c]	0.44	0.54

[a]This work. [b]From ref *52*. [c]From ref *53*.

Factors Influencing the Cysteine pK_a Values. The results presented thus far highlight two important factors that influence the cysteine pK_a values. First, the average values of ∼7.15 for Cys14 and ∼7.7 for Cys11 observed in the C11A and C14A mutants, respectively, are both substantially lower than the typical value of 9−10 for a cysteine thiol in an unstructured peptide in solution. The most significant factor likely contributing to this stabilization is their location at the positive end (N-terminus) of the macrodipole of α-helix 1, which in model peptides can lower the cysteine thiol pK_a to ∼7.5 (*59*, *60*). As shown in Figure 6A, Cys14 is more precisely positioned in the first turn of the helix, which may partially explain its greater stabilization compared with that of Cys11 located in the more flexible loop preceding the helix.

The dramatic and opposite shift of the pK_a values for the individual cysteines in the mutants versus the wild-type protein suggests the residues interact strongly in the wild-type protein and is consistent with the observation that the β-^{13}C nuclei of both cysteines detect both ionizations. The latter observation is reminiscent of the pH-dependent ^{13}C NMR titration behavior of the redox active CXXC motif in *E. coli* thioredoxin (Trx) (*52*, *53*). However, the titration profiles for the two cysteines in each protein show distinctive differences (Table 2) that may reflect differences in their structural constraints (Figure 6). With Trx, the chemical shift change ($\Delta\delta$) associated with each of the two pK_a values is relatively large for Cys32, but much smaller for Cys35 (Table 2), which lies between Cys32 and Asp26 (Figure 6B). A large body of data, including the proximity of the structurally well-constrained cysteines, led to the suggestion of proton sharing as an explanation for why both pK_a values are sensed by both cysteines in Trx (*52*, *61*). However, the alternative hypothesis that the two ionizations represent the successive microscopic ionizations of Cys32 and Asp26 in a negative cooperative interaction (*53*) seems more consistent with the similarly large $\Delta\delta$ values for both pK_a values observed by Cys32 and the relatively small $\Delta\delta$ values for Cys35 that would "feel" the developing negative charge on both Cys32 and Asp26 in this scheme but would not undergo ionization itself. This latter hypothesis is also consistent with the occurrence of proton sharing to some extent among all three residues in the singly ionized protein. With NmerA, the titration behavior is significantly different. Here, the $\Delta\delta$ values are much larger for the first pK_a for both cysteines than the $\Delta\delta$ values associated with the second pK_a in both (Table 2). Taken alone, this combination of $\Delta\delta$ changes could be explained equally well by a microscopic ionization model involving Cys14 and Cys11 in

a negative cooperative interaction or a successive ionization model with direct proton sharing between the cysteine sulfurs in the singly ionized protein. However, the distinctively different $\Delta\varepsilon_{240}$ values observed for ionization of Cys14 and Cys11 are inconsistent with the microscopic ionization model, which would predict similar $\Delta\varepsilon$ values for the two phases if half of each were ionizing in each phase. In addition, the structural models derived from our NMR constraints do not support direct proton sharing between the cysteine thiols either. However, they do suggest an alternative interaction (Figure 6A) that could affect the thiol pK_a in the absence of proton sharing. Only two sets of NOEs define the position of Cys14 relative to the loop containing Cys11: NOEs between the β-protons of Cys14 and the β-protons of Met9 giving distances of 2.6−3.5 Å and, more importantly, NOEs between the Cys11 N−H proton and the Cys14 β-protons giving distances of 3.2 and 4.5 Å. The rest of the loop structure is primarily defined by angle and NOE distance constraints between residues within the loop itself. These constraints suggest the loop is much more flexible in NmerA and yield models with a mean S−S distance of ~6.1 Å (range of 3.6−7.6 Å) consistent with its functional role in Hg^{2+} binding rather than oxidation/reduction. While this is too long for direct proton sharing, the distance constraints for the Cys11 N−H and Cys14 β-protons frequently place the Cys11 N−H bond in a position to provide a dipolar interaction with the Cys14 thiolate anion (Figure 6A). Development of substantial $\delta-$ charge on the Cys11 amide nitrogen in the singly ionized protein may be responsible for the large $\Delta\delta$ value associated with the first pK_a observed for the β-^{13}C carbon of Cys11.

Although the helix dipole and loop structure appear to be major factors influencing the cysteine pK_a values, there are also two conserved amino acid side chains, His17 and Tyr62, that reside near the Cys14 thiol and could provide additional stabilization of the thiolate anion. To examine the influence of these residues on the thiol ionizations, we separately introduced H17N and Y62F mutations.

His17. As noted above in Figure 3, His17 is located one turn from Cys14 in α-helix 1 and is too distant to participate directly as an acid or base catalyst to protonate or deprotonate the cysteine thiol. However, with an average distance of ~8 Å between the sulfur and the nearest atom of the imidazole ring observed in the calculated structures, it is plausible that the protonated His could provide some electrostatic stabilization of the thiolate anion that would be abolished upon mutation of His to a neutral residue. Since many of the calculated structures for reduced NmerA place the Tyr62 hydroxyl group within hydrogen bonding distance of His17 Nδ, we replaced His with Asn to remove the charge while retaining heteroatoms at the δ-positions for potential hydrogen bonding. Evidence that the Cys14 side chain can detect the charge state of His17 comes from the observation of a single pK_a of 6.7 in the ^{13}C chemical shift versus pH data for the Cys14 β-carbon in the oxidized (disulfide) form of wild-type NmerA, and the disappearance of that sensitivity in the H17N mutant (Figure 7). However, the magnitude of the shift is quite small (~0.3 ppm vs ~1.4 ppm associated with ionization of Cys14 in the reduced wild-type protein), suggesting the electrostatic interaction is fairly weak. Consistent with this, the pH titrations of the reduced H17N mutant revealed only minor increases (0.2−0.4 pH unit) in the cysteine pK_a values (Table 1 and Figure S4B of the Supporting Information). In further agreement, the pK_a of His17 in reduced wild-type NmerA was previously determined to be ~7.0 (*62*), only slightly elevated from the value

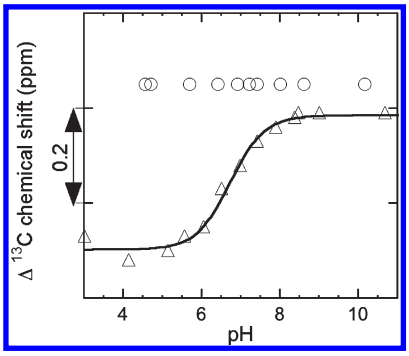

FIGURE 7: Change in the ^{13}C NMR chemical shifts for the β-carbon of Cys14 as a function of pH in (△) oxidized wild-type NmerA and (○) oxidized H17N mutant NmerA. No changes in chemical shift for the Cys11 β-carbon were observed in either protein.

of 6.7 in the oxidized protein by the presence of the Cys14 thiolate anion. Thus, His17 does not play a major role in modulating the basicity or reactivity of the cysteine thiols. Despite this, as will be described elsewhere, this uniquely conserved residue is important for kinetically efficient transfer of Hg^{2+} from NmerA to the catalytic core.

Tyr62. While His17 is constrained by helix 1 to remain some distance from the Cys14 thiol, the aromatic ring of Tyr62 is less stringently constrained. The Cα−Cβ bond of Tyr62 is oriented by the short well-constrained loop 5 placing the aromatic ring in a crevice between loop 5 and the first two turns of helix 1. However, the lack of detectable NOEs between the Tyr62 ring protons and any other residues is consistent with the side chain undergoing nanosecond rotational fluctuations about its Cα−Cβ and Cβ−Cγ bonds. As observed in the 20 lowest-energy structures, these rotations allow the Tyr62 OH group to approach either Nδ of His17 or the Cys14 sulfur at the extremes of its range of motion and suggest Tyr62 may afford some stabilization of the Cys14 thiolate through a dipolar interaction. One indication that Tyr62 interacts with the Cys14 sulfur is the observation that the pK_a value for the tyrosines[3] in the oxidized wild-type NmerA is shifted downward by ~1 pH unit relative to that in the reduced protein (Table 1); i.e., the absence of the negatively charged thiolate allows ionization of the Tyr OH at a lower pH. To examine the effect in reverse, the polar effects of the hydroxyl group were removed by replacement of tyrosine with phenylalanine, and the pK_a values for the Y62F cysteine thiols were obtained using the ^{13}C NMR and ΔA_{240} approaches described above. As shown in Figure 4B, both cysteine β-carbons in the Y62F mutant exhibit two ionizations with pK_a values of ~6.7 and 10, an upward shift of 0.8−1 pH unit for both pK_a values relative to those in the wild-type protein. Similar shifts for the cysteine pK_a values were obtained from the ΔA_{240} titration, while the pK_a for the remaining tyrosine (Tyr35) changed very little (Table 1 and Figure S5 of the Supporting Information). The simplest interpretation of these results is that in the absence of the stabilizing polar interaction of Tyr62 with Cys14, both cysteine pK_a values are increased, but Cys14 still has the lower value. Curiously, however, the magnitudes of the $\Delta\delta$ values associated with each pK_a for the two

[3]Of interest here, both Tyr35 and Tyr62 contribute to the absorbance change at high pH and therefore must have the same pK_a values within the limits of detection in both the oxidized and reduced forms of the protein. Because Tyr35 is located in loop 3 and resides in the vicinity of Cys11, this suggests that it too may contribute to stabilization of the cysteine thiolates via an interaction with Cys11.

cysteines as well as the $\Delta\varepsilon_{240}$ values are quite different from those observed for the wild-type protein (Table 1). Both the much lower $\Delta\varepsilon_{240}$ (similar to that observed for Cys11 in the C14A mutant) for the first pK_a and the much larger fraction of the total $\Delta\delta$ for Cys11 associated with the first pK_a suggest Cys11 may actually have the lower pK_a in the Y62F mutant. A higher pK_a for Cys14 would be consistent with a more hydrophobic environment resulting from the loss of the polar Tyr62 OH group. Regardless of which interpretation is correct, of most significance is the fact that Tyr62 does indeed stabilize the cysteine thiolate anions and would be expected to influence the affinity and reactivity of the protein toward Hg^{2+} binding and transfer. Further examination of the effects of this mutation on these properties of NmerA will be described elsewhere.

Conclusions. The solution structures of NmerA with and without Hg^{2+} determined here provide the structural framework for investigation of the features contributing to its specificity and balancing roles in mediating mercuric ion transfers. The dominant feature of mercuric ion transfer is the alternating function of the cysteine thiols that are mediated by their pK_a values. We describe both the structural and thermodynamic features that contribute to the modulation of these metal binding cysteine pK_a values.

ACKNOWLEDGMENT

We thank Felician Dancea for help performing energy minimization of the calculated structures and preparing Table S1 of the Supporting Information (structural statistics).

SUPPORTING INFORMATION AVAILABLE

$^1H-^{15}N$ FHSQC spectrum for reduced NmerA with arrows to altered peaks in HgNmerA (Figure S1), structural statistics for both structures together with a brief description (Table S1), ε_{240} versus pH for wild-type, C11A, and C14A NmerA from the second approach (Figure S2), ε_{293} versus pH for wild-type and Y62F NmerA (Figure S3), Cβ-[^{13}C]cysteine chemical shifts versus pH for C14A, C11A, and H17N NmerA mutants (Figure S4), and ε_{240} versus pH for Y62F NmerA (Figure S5). This material is available free of charge via the Internet at http://pubs.acs.org.

REFERENCES

1. Foster, T. J. (1983) Plasmid-determined resistance to antimicrobial drugs and toxic metal ions in bacteria. *Microbiol. Rev. 47*, 361–409.
2. Vallee, B. L., and Ulmer, D. D. (1972) Biochemical effects of mercury, cadmium, and lead. *Annu. Rev. Biochem. 41*, 91–128.
3. O'Halloran, T. V., and Culotta, V. C. (2000) Metallochaperones, an intracellular shuttle service for metal ions. *J. Biol. Chem. 275*, 25057–25060.
4. Rensing, C., Ghosh, M., and Rosen, B. P. (1999) Families of soft-metal-ion-transporting ATPases. *J. Bacteriol. 181*, 5891–5897.
5. Miller, S. (1999) Bacterial detoxification of Hg(II) and organomercurials. in Essays in Biochemistry (Ballou, D. P., Ed.) pp 17−30, Princeton University Press, Princeton, NJ.
6. Barkay, T., Miller, S. M., and Summers, A. O. (2003) Bacterial mercury resistance from atoms to ecosystems. *FEMS Microbiol. Rev. 27*, 355–384.
7. Silver, S. (1996) Bacterial resistances to toxic metal ions: A review. *Gene 179*, 9–19.
8. Silver, S., and Phung, L. T. (1996) Bacterial heavy metal resistance: New surprises. *Annu. Rev. Microbiol. 50*, 753–789.
9. Mukhopadhyay, R., and Rosen, B. P. (2002) Arsenate reductases in prokaryotes and eukaryotes. *Environ. Health Perspect. 110* (Suppl. 5), 745–748.
10. Cheesman, B. V., Arnold, A. P., and Rabenstein, D. L. (1988) Nuclear magnetic resonance studies of the solution chemistry of metal complexes. 25. $Hg(thiol)_3$ complexes and Hg(II)-thiol ligand exchange kinetics. *J. Am. Chem. Soc. 110*, 6359–6364.
11. Schottel, J. L. (1978) The mercuric and organomercurial detoxifying enzymes from a plasmid-bearing strain of *Escherichia coli*. *J. Biol. Chem. 253*, 4341–4349.
12. Brown, N. L. (1985) Bacterial resistance to mercury: Reductio ad absurdum? *Trends Biochem. Sci. 10*, 400–403.
13. Summers, A. O. (1986) Organization, expression, and evolution of genes for mercury resistance. *Annu. Rev. Microbiol. 40*, 607–634.
14. Fox, B., and Walsh, C. T. (1982) Mercuric reductase. Purification and characterization of a transposon-encoded flavoprotein containing an oxidation-reduction-active disulfide. *J. Biol. Chem. 257*, 2498–2503.
15. Fox, B. S., and Walsh, C. T. (1983) Mercuric reductase: Homology to glutathione reductase and lipoamide dehydrogenase. Iodoacetamide alkylation and sequence of the active site peptide. *Biochemistry 22*, 4082–4088.
16. Brown, N. L., Ford, S. J., Pridmore, R. D., and Fritzinger, D. C. (1983) Nucleotide sequence of a gene from the *Pseudomonas* transposon Tn*501* encoding mercuric reductase. *Biochemistry 22*, 4089–4095.
17. Williams, C. H., Arscott, L. D., Muller, S., Lennon, B. W., Ludwig, M. L., Wang, P. F., Veine, D. M., Becker, K., and Schirmer, R. H. (2000) Thioredoxin reductase two modes of catalysis have evolved. *Eur. J. Biochem. 267*, 6110–6117.
18. Miller, S. M., Moore, M. J., Massey, V., Williams, C. H., Jr., Distefano, M. D., Ballou, D. P., and Walsh, C. T. (1989) Evidence for the participation of Cys558 and Cys559 at the active site of mercuric reductase. *Biochemistry 28*, 1194–1205.
19. Moore, M. J., and Walsh, C. T. (1989) Mutagenesis of the N- and C-terminal cysteine pairs of Tn*501* mercuric ion reductase: Consequences for bacterial detoxification of mercurials. *Biochemistry 28*, 1183–1194.
20. Distefano, M. D., Au, K. G., and Walsh, C. T. (1989) Mutagenesis of the redox-active disulfide in mercuric ion reductase: Catalysis by mutant enzymes restricted to flavin redox chemistry. *Biochemistry 28*, 1168–1183.
21. Distefano, M. D., Moore, M. J., and Walsh, C. T. (1990) Active site of mercuric reductase resides at the subunit interface and requires Cys135 and Cys140 from one subunit and Cys558 and Cys559 from the adjacent subunit: Evidence from in vivo and in vitro heterodimer formation. *Biochemistry 29*, 2703–2713.
22. Miller, S. M., Massey, V., Williams, C. H., Jr., Ballou, D. P., and Walsh, C. T. (1991) Communication between the active sites in dimeric mercuric ion reductase: An alternating sites hypothesis for catalysis. *Biochemistry 30*, 2600–2612.
23. Moore, M. J., Miller, S. M., and Walsh, C. T. (1992) C-Terminal cysteines of Tn*501* mercuric ion reductase. *Biochemistry 31*, 1677–1685.
24. Schiering, N., Kabsch, W., Moore, M. J., Distefano, M. D., Walsh, C. T., and Pai, E. F. (1991) Structure of the detoxification catalyst mercuric ion reductase from *Bacillus* sp. strain RC607. *Nature 352*, 168–172.
25. Engst, S., and Miller, S. M. (1998) Rapid reduction of Hg(II) by mercuric ion reductase does not require the conserved C-terminal cysteine pair using $HgBr_2$ as the substrate. *Biochemistry 37*, 11496–11507.
26. Engst, S., and Miller, S. M. (1999) Alternative routes for entry of HgX_2 into the active site of mercuric ion reductase depend on the nature of the X ligands. *Biochemistry 38*, 3519–3529.
27. Ledwidge, R., Patel, B., Dong, A., Fiedler, D., Falkowski, M., Zelikova, J., Summers, A. O., Pai, E. F., and Miller, S. M. (2005) NmerA, the metal binding domain of mercuric ion reductase, removes Hg^{2+} from proteins, delivers it to the catalytic core, and protects cells under glutathione-depleted conditions. *Biochemistry 44*, 11402–11416.
28. Arnesano, F., Banci, L., Bertini, I., Ciofi-Baffoni, S., Molteni, E., Huffman, D. L., and O'Halloran, T. V. (2002) Metallochaperones and metal-transporting ATPases: A comparative analysis of sequences and structures. *Genome Res. 12*, 255–271.
29. Miller, S. M. (1999) Construction of separate expression vectors for the catalytic core and the N-terminal metal binding domain of Tn*501* mercuric ion reductase. In Flavins and Flavoproteins 1999 (Ghisla, S., Kroneck, P., Macheroux, P., and Sund, H., Eds.) pp 863−870, Agency for Scientific Publications, Berlin.
30. Cheng, H., Westler, W. M., Xia, B., Oh, B. H., and Markley, J. L. (1995) Protein expression, selective isotopic labeling, and analysis of hyperfine-shifted NMR signals of Anabaena 7120 vegetative [2Fe-2S]ferredoxin. *Arch. Biochem. Biophys. 316*, 619–634.
31. Kay, L. E., Marion, D., and Bax, A. (1989) Practical aspects of 3D heteronuclear NMR of proteins. *J. Magn. Reson. 84*, 72–84.
32. Kay, L. E., Ikura, M., Tschudin, R., and Bax, A. (1990) Three-dimensional triple-resonance NMR spectroscopy of isotopically enriched proteins. *J. Magn. Reson. 89*, 496–514.

33. Grzesiek, S., and Bax, A. (1992) Correlating backbone amide and side chain resonances in larger proteins by multiple relayed triple resonance NMR. *J. Am. Chem. Soc. 114*, 6291–6293.
34. Grzesiek, S., and Bax, A. (1993) Amino acid type determination in the sequential assignment procedure of uniformly $^{13}C/^{15}N$-enriched proteins. *J. Biomol. NMR 3*, 185–204.
35. Vuister, G. W., and Bax, A. (1993) Quantitative J Correlation: A new approach for measuring homonuclear three bond $J(H^NH^a)$ coupling constants in ^{15}N-enriched proteins. *J. Am. Chem. Soc. 115*, 7772–7777.
36. Neri, D., Szyperski, T., Otting, G., Senn, H., and Wuthrich, K. (1989) Stereospecific nuclear magnetic resonance assignments of the methyl groups of valine and leucine in the DNA-binding domain of the 434 repressor by biosynthetically directed fractional ^{13}C labeling. *Biochemistry 28*, 7510–7516.
37. Piotto, M., Saudek, V., and Sklenar, V. (1992) Gradient-tailored excitation for single-quantum NMR spectroscopy of aqueous solutions. *J. Biomol. NMR 2*, 661–665.
38. Eccles, C., Guntert, P., Billeter, M., and Wuthrich, K. (1991) Efficient analysis of protein 2D NMR spectra using the software package EASY. *J. Biomol. NMR 1*, 111–130.
39. Guntert, P., Mumenthaler, C., and Wuthrich, K. (1997) Torsion angle dynamics for NMR structure calculation with the new program DYANA. *J. Mol. Biol. 273*, 283–298.
40. Taylor, N. J., and Carty, A. J. (1977) Nature of Hg^{2+}-L-cysteine complexes implicated in mercury biochemistry. *J. Am. Chem. Soc. 99*, 6143–6145.
41. Wright, J. G., Tsang, H.-T., Penner-Hahn, J. E., and O'Halloran, T. V. (1990) Coordination chemistry of the Hg-MerR metalloregulatory protein: Evidence for a novel tridentate Hg-cysteine receptor site. *J. Am. Chem. Soc. 112*, 2434–2435.
42. Brünger, A. T., Adams, P. D., Clore, G. M., DeLano, W. L., Gros, P., Grosse-Kunstleve, R. W., Jiang, J. S., Kuszewski, J., Nilges, M., Pannu, N. S., Read, R. J., Rice, L. M., Simonson, T., and Warren, G. L. (1998) Crystallography & NMR system: A new software suite for macromolecular structure determination. *Acta Crystallogr. D54* (Part 5), 905–921.
43. Linge, J. P., Williams, M. A., Spronk, C. A., Bonvin, A. M., and Nilges, M. (2003) Refinement of protein structures in explicit solvent. *Proteins 50*, 496–506.
44. Steele, R. A., and Opella, S. J. (1997) Structures of the reduced and mercury-bound forms of MerP, the periplasmic protein from the bacterial mercury detoxification system. *Biochemistry 36*, 6885–6895.
45. Bersch, B., Rossy, E., Coves, J., and Brutscher, B. (2003) Optimized set of two-dimensional experiments for fast sequential assignment, secondary structure determination, and backbone fold validation of $^{13}C/^{15}N$-labelled proteins. *J. Biomol. NMR 27*, 57–67.
46. Rossy, E., Champier, L., Bersch, B., Brutscher, B., Blackledge, M., and Coves, J. (2004) Biophysical characterization of the MerP-like amino-terminal extension of the mercuric reductase from *Ralstonia metallidurans* CH34. *J. Biol. Inorg. Chem. 9*, 49–58.
47. Banci, L., Bertini, I., Ciofi-Baffoni, S., Huffman, D. L., and O'Halloran, T. V. (2001) Solution structure of the yeast copper transporter domain Ccc2a in the apo and Cu(I)-loaded states. *J. Biol. Chem. 276*, 8415–8426.
48. Arnesano, F., Banci, L., Bertini, I., Huffman, D. L., and O'Halloran, T. V. (2001) Solution structure of the Cu(I) and apo forms of the yeast metallochaperone, Atx1. *Biochemistry 40*, 1528–1539.
49. Rossy, E., Seneque, O., Lascoux, D., Lemaire, D., Crouzy, S., Delangle, P., and Coves, J. (2004) Is the cytoplasmic loop of MerT, the mercuric ion transport protein, involved in mercury transfer to the mercuric reductase? *FEBS Lett. 575*, 86–90.
50. Lindley, H. (1960) A study of the kinetics of the reaction between thiol compounds and choloracetamide. *Biochem. J. 74*, 577–584.
51. Kallis, G. B., and Holmgren, A. (1980) Differential reactivity of the functional sulfhydryl groups of cysteine-32 and cysteine-35 present in the reduced form of thioredoxin from *Escherichia coli*. *J. Biol. Chem. 255*, 10261–10265.
52. Jeng, M. F., Holmgren, A., and Dyson, H. J. (1995) Proton sharing between cysteine thiols in *Escherichia coli* thioredoxin: Implications for the mechanism of protein disulfide reduction. *Biochemistry 34*, 10101–10105.
53. Chivers, P. T., Prehoda, K. E., Volkman, B. F., Kim, B. M., Markley, J. L., and Raines, R. T. (1997) Microscopic pKa values of *Escherichia coli* thioredoxin. *Biochemistry 36*, 14985–14991.
54. Benesch, R. E., and Benesch, R. (1955) The acid strength of the -SH group in cysteine and related compounds. *J. Am. Chem. Soc. 77*, 5877–5881.
55. Graminski, G. F., Kubo, Y., and Armstrong, R. N. (1989) Spectroscopic and kinetic evidence for the thiolate anion of glutathione at the active site of glutathione S-transferase. *Biochemistry 28*, 3562–3568.
56. Edelhoch, H. (1967) Spectroscopic determination of tryptophan and tyrosine in proteins. *Biochemistry 6*, 1948–1954.
57. Atkins, W. M., Wang, R. W., Bird, A. W., Newton, D. J., and Lu, A. Y. (1993) The catalytic mechanism of glutathione S-transferase (GST). Spectroscopic determination of the pKa of Tyr-9 in rat α1-1 GST. *J. Biol. Chem. 268*, 19188–19191.
58. Powlowski, J., and Sahlman, L. (1999) Reactivity of the two essential cysteine residues of the periplasmic mercuric ion-binding protein, MerP. *J. Biol. Chem. 274*, 33320–33326.
59. Kortemme, T., and Creighton, T. E. (1995) Ionisation of cysteine residues at the termini of model α-helical peptides. Relevance to unusual thiol pKa values in proteins of the thioredoxin family. *J. Mol. Biol. 253*, 799–812.
60. Wada, A. (1976) The α-helix as an electric macro-dipole. *Adv. Biophys.*, 1–63.
61. Pearl, L., and Blundell, T. (1984) The active site of aspartic proteinases. *FEBS Lett. 174*, 96–101.
62. Shimba, N., Serber, Z., Ledwidge, R., Miller, S. M., Craik, C. S., and Dötsch, V. (2003) Quantitative identification of the protonation state of histidines in vitro and in vivo. *Biochemistry 42*, 9227–9234.
63. Koradi, R., Billeter, M., and Wuthrich, K. (1996) MOLMOL: A program for display and analysis of macromolecular structures. *J. Mol. Graphics 14* (51−55), 29–32.
64. Pettersen, E. F., Goddard, T. D., Huang, C. C., Couch, G. S., Greenblatt, D. M., Meng, E. C., and Ferrin, T. E. (2004) UCSF Chimera: A visualization system for exploratory research and analysis. *J. Comput. Chem. 25*, 1605–1612.
65. DeLano, W. L. (2002) The PyMOL Molecular Graphics System, DeLano Scientific, San Carlos, CA.